







Received 8 March 2024; revised 18 May 2024; accepted 15 July 2024. Date of publication 18 July 2024; date of current version 9 August 2024. The review of this article was arranged by Associate Editor Shafiq Odhano.

Digital Object Identifier 10.1109/OJIA.2024.3430861

# Investigating PWM-Induced Iron Losses: Measurements and Estimation Models up to 350 kHz Switching Frequency

LUIGI DANILO TORNELLO <sup>1</sup> (Member, IEEE), SILVIO VASCHETTO <sup>2</sup> (Senior Member, IEEE), EMMANUEL B. AGAMLOH <sup>3</sup> (Senior Member, IEEE), GIACOMO SCELBA <sup>1</sup> (Senior Member, IEEE), GIULIO DE DONATO <sup>4</sup> (Senior Member, IEEE), AND ANDREA CAVAGNINO <sup>2</sup> (Fellow, IEEE)

<sup>1</sup>Department of Electrical, Electronic and Computer Engineering, University of Catania, 95125 Catania, Italy

<sup>2</sup>Politecnico di Torino, Dipartimento Energia 'G. Ferraris', 10129 Torino, Italy

<sup>3</sup>Department of Electrical and Computer Engineering, Baylor University, Waco, TX 76798-7151 USA

<sup>4</sup>Department of Astronautical, Electrical and Energy Engineering, Sapienza University of Rome, 00184 Rome, Italy

CORRESPONDING AUTHOR: ANDREA CAVAGNINO (e-mail: andrea.cavagnino@polito.it).

This work was supported by «TURBO: the Next 100 000+r/min Synchronous Reluctance Motor Drives» Project—funded by European Union—Next Generation EU within the PRIN 2022 Program (D.D. 104 - 02/02/2022 Ministero dell'Università e della Ricerca).

**ABSTRACT** This article deals with the investigation of iron losses in toroidally wound laminated magnetic cores excited with wide-bandgap-device-based power electronic converters. The study aims to analyze the impact of selected pulsewidth modulation voltages on the iron losses, through an extensive experimental measurement campaign. In particular, four toroidal specimens made of different magnetic materials are supplied by pulsewidth-modulated voltage waveforms with switching frequencies ranging from 1 to 350 kHz and different deadtimes. Test campaigns have been conducted with the dual objectives of critically reviewing an engineering method proposed in the prior literature for predicting iron losses under distorted voltage waveforms. Additionally, the aim is to extend this estimation model to accommodate the highest frequencies currently employed in high-speed ac motor drives equipped with wide-bandgap semiconductor power converters.

**INDEX TERMS** AC sinusoidal supply, eddy currents, high-speed machines, iron losses, magnetic hysteresis, measurements, modeling, pulsewidth modulation (PWM), soft magnetic material, wide-bandgap (WBG) device-based inverters.

## I. INTRODUCTION

In recent years, high-speed electrical machines have been increasingly utilized in various high-power density applications. Examples include high-speed spindles (300 000 r/min), microturbines (120 000 r/min), air compressors and air blowers (80 000 r/min), as well as traction motors (35 000 r/min) [1], [2]. At these rotational speeds, the supply frequencies exceed 1 kHz, requiring pulsewidth modulation (PWM) voltages with switching frequencies above 50 kHz in order to obtain reasonable current ripples and guarantee a stable control [3].

Wide-bandgap (WBG) semiconductor power devices, such as silicon carbide (SiC) and gallium nitride, feature very short commutation transients and can be hard switched at frequencies well above 50 kHz [4]. Unfortunately, extra losses due to

the high switching frequencies are unavoidable in the electrical machine, especially the iron loss, which represents a significant portion of the total losses at high rotational speeds [5]. Therefore, the accurate prediction of iron losses at both high fundamental and switching frequencies becomes a critical aspect for the successful design of high-speed electrical machines, particularly when the magnetic cores are composed of high-grade thin magnetic laminations.

In catalogs, magnetic laminations are typically characterized solely under “pure” sinusoidal excitation. Consequently, technical publications providing the watt/kilogram data under PWM voltage supply or, even better, practical estimation models are particularly welcome to designers tasked with designing machines from the scratch [6], [7], [8].

The history of iron loss estimation in ferromagnetic materials dates back many decades when empirical models were introduced for purely sinusoidal flux density waves. These models were developed based on the significant contributions of Steinmetz and Bertotti [9], [10]. They differ in how they subdivide the overall iron losses into their main contributions and their dependence on the fundamental frequency and flux density. Various models have also been developed to address PWM-induced iron losses. However, in most cases, these models are complex and impractical for immediate use by electrical machine designers, especially when dealing with WBG-based inverters [11], [12], [13], [14], [15]. That is why, the authors are hereby proposing simple yet accurate formulations to calculate iron losses under ultrahigh switching frequency PWM. The main goal of this research work is to investigate iron losses in magnetic laminations under extremely fast switching conditions. Specifically, the article is focused on the experimental measurement of iron losses in four toroidally laminated cores made from magnetic materials with significant differences in alloy composition, thickness, and dimensions. Two of the tested specimens have been realized directly using the stator magnetic cores of high-power density traction motors.

An SiC H-bridge inverter, exploring a wide range of switching frequencies and deadtimes, feeds all the cores. The results are then processed to reevaluate the applicability of the analytical model initially introduced in [16] and, more recently, in [17] for predicting iron losses under PWM excitation at high switching frequencies. In particular, the model has been validated in high fundamental and switching frequency ranges: 50–2000 Hz and 1–350 kHz, respectively.

### A. ARTICLE STRUCTURE

This article summarizes a research activity conducted over the past two years. Therefore, before going into the details, it is beneficial to outline the article’s structure and the logical sequence of the development presentation. The rest of this article is organized as follows. Sections II and III detail with the test campaigns conducted and the challenges that were addressed to achieve the accurate PWM-induced iron loss measurements up to 350 kHz switching frequency. In Section IV, the iron losses of two samples are presented and discussed for fundamental frequencies of 50 and 200 Hz. In Section V, these measurements have been used to demonstrate that a physical-based estimation loss model developed by the authors more than 20 years ago is not applicable above 5 kHz of switching frequency. Contextually, the experimental observations were also used to extend the model validity by introducing a new coefficient applied to the eddy current losses, which is identified with a data-fitting approach. The final validation of the new proposed model is presented in Section VI, using the results coming from the second test campaign carried out at high fundamental frequencies. Section VII presents a specific design-oriented iron loss model, suitable for estimations up to 2000 Hz and 350 kHz of fundamental and switching frequencies, together with a fast identification

TABLE 1. Sample #1 Specifications (M800-50A, FeSi Alloy)

Primary winding turns, $N_1$	107
Secondary winding turns, $N_2$	107
Lamination thickness, (mm)	0.5
Radial thickness, (mm)	40
Weight, (kg)	3.55
Cross-sectional area, (mm <sup>2</sup> )	900



TABLE 2. Sample #2 Specifications (VACOFLUX 50, FeCo Alloy)

Primary winding turns, $N_1$	73
Secondary winding turns, $N_2$	66
Lamination thickness, (mm)	0.35
Radial thickness, (mm)	17.5
Weight, (kg)	1.62
Cross-sectional area, (mm <sup>2</sup> )	457



TABLE 3. Sample #3 Specifications (NO30-16, FeSi Alloy)

Primary winding turns, $N_1$	120
Secondary winding turns, $N_2$	120
Lamination thickness, (mm)	0.3
Radial thickness, (mm)	10
Weight, (kg)	2.77
Cross-sectional area, (mm <sup>2</sup> )	447



TABLE 4. Sample #4 Specifications (NO27-15, FeSi Alloy)

Primary winding turns, $N_1$	24 (12)
Secondary winding turns, $N_2$	24 (12)
Lamination thickness, (mm)	0.27
Radial thickness, (mm)	13.2
Weight, (kg)	9.51
Cross-sectional area, (mm <sup>2</sup> )	2363



procedure of the model’s unknowns, dedicated to designers who have a test structure available. Finally, Section VIII concludes this article.

## II. SAMPLES DESCRIPTION AND METHODOLOGY

An experimentally based approach is proposed to collect data for quantifying the impact of the switching frequency and deadtime on losses in laminated cores. Additionally, practical estimation loss models under PWM supply are developed using the gathered data.

In this research work, four toroidal cores of different materials and dimensions were tested. They are presented in Tables 1–4, along with the material type and main dimensions. Note that different materials, such as silicon–iron (FeSi) and cobalt–iron (FeCo) alloys, as well as different grades and geometries, have been considered to ensure maximum generality in the analysis. From this perspective, the assembly

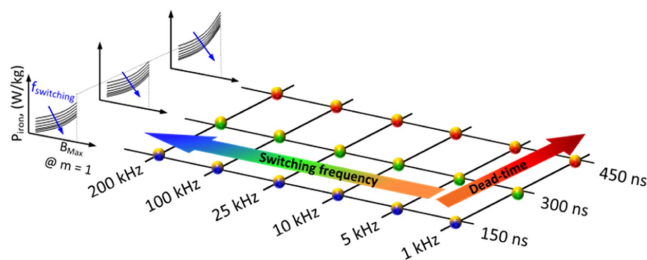


**FIGURE 1.** Switching frequency versus deadtime with a fundamental harmonic of PWM voltage at the considered fundamental frequency of 50 or 200 Hz.

of the samples also differs: sample #1 is made up of loose toroidal-shaped magnetic sheets, while sample #2 is produced by assembling loose stator laminations of a real machine designed for aerospace applications. Sample #3 and sample #4 consist of existing stator cores of high-performance traction motors, manufactured using backlack-coated laminations.

The sample #2 and the stator cores #3 and #4 have been toroidally wound, positioning the sensing winding in the bottom of the slot and, consequently, testing the material in their yoke. Due to their big yoke cross sections, suitable turn numbers for the primary and secondary winding have been selected in order to respect the current and voltage limits of the available test rig when the fundamental frequency increases. In particular, for the sample #4, the windings are not overlapped, limiting the resonance phenomenon at the higher switching frequencies, with a 24/24 turn ratio for the 50–400 Hz tests and a 12/12 turn ratio for the 1000–2000 Hz tests.

The overall experimentally based approach has been subdivided into two main stages.

1) *The low fundamental frequency analysis:* An initial test campaign has been conducted on the sample #1 and sample #2, following the switching frequency/deadtime “mapping,” as shown in Fig. 1, at both 50 and 200 Hz fundamental frequencies. The objectives of these measurements are not only to evaluate the impacts of specific PWM voltage waveform characteristics on iron losses but also to verify the applicability and potential refinement of an engineering loss prediction method under the PWM supply previously proposed by the authors.

Given the low fundamental frequency, the switching frequency was varied within the 1–200 kHz range.

2) *The high fundamental frequency analysis* involves testing all four samples with a deadtime equal to 150 ns, fundamental frequencies ranging from 400 to 2000 Hz and switching frequencies from 50 up to 350 kHz. The primary objective of this analysis is a critical discussion of the measurement results and their application in the estimation models developed based on the low fundamental frequency data.

### III. MEASUREMENTS SETUP AND PROCEDURES

The test rig used to measure the iron losses is shown in Fig. 2. It includes an SiC H-bridge inverter powered by a

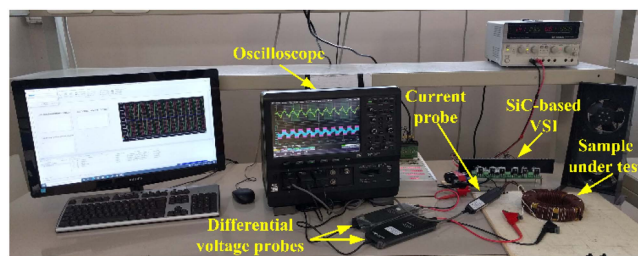


**FIGURE 2.** Test rig used for the iron loss measurements.

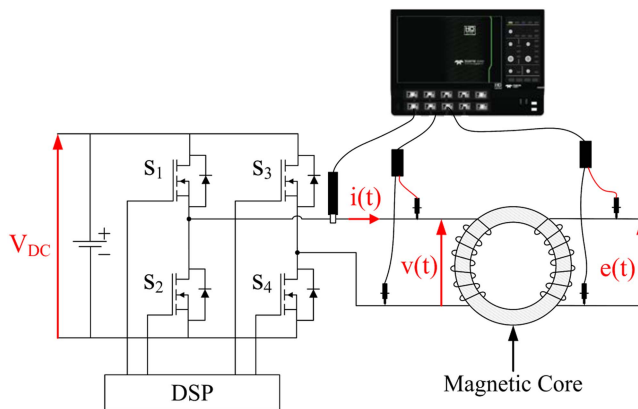


**FIGURE 3.** Measurement layout setup.

high-voltage dc power supply, with its output terminals connected to the primary winding of the toroidal cores under test. Following the scheme reported in Fig. 3, the primary current  $i(t)$  magnetizes the core at the desired magnetic field strength, while the secondary sensing winding is employed to measure the induced voltage  $e(t)$ . Flux density and iron losses in the magnetic core are obtained by elaborating the measured primary current and secondary voltage [18]. Note that the specific iron losses in (W/kg) represent the active power associated with the instantaneous power  $p(t) = N_1 e(t) i(t) / N_2$ , divided by the specimen weight.

An example of the three time-variant signals to be measured is illustrated in Fig. 4. Observing the figure and considering that, in the conducted tests, the switching frequencies are much higher than 20–25 kHz, it becomes evident that iron losses cannot be measured with standard commercially available power meters. Only data loggers or oscilloscopes with adequate sampling capability and qualified to measure both the fundamental harmonic and rms values of electrical quantities, such as active power, can be employed.

The experiments were conducted by setting the magnitude and frequency of the reference fundamental voltages using an STM32 Nucleo G474RE controller board. On the same board, the switching frequencies and deadtimes of the modulation strategy can be modified. The modulation utilized is a unipolar sine-triangle PWM to avoid minor hysteresis loops and, consequently, further iron losses—see Fig. 5. In the absence of minor loops, the “distance” between the red and black

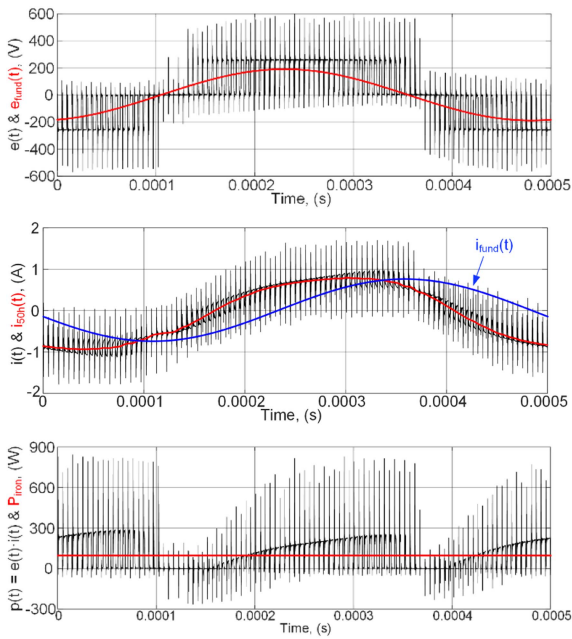


**FIGURE 4.** Acquired signals for sample #1 at fundamental frequency = 2000 Hz, switching frequency = 100 kHz, and  $m_i = 0.9$ . From top to bottom: the induced voltage  $e(t)$ , magnetizing current  $i(t)$ , and instantaneous power  $p(t)$ . In black: full spectrum waveforms; in red: fundamental induced voltage, magnetizing current reconstructed using its first 50 harmonics, and active power from the instantaneous power. In blue: fundamental magnetizing current.

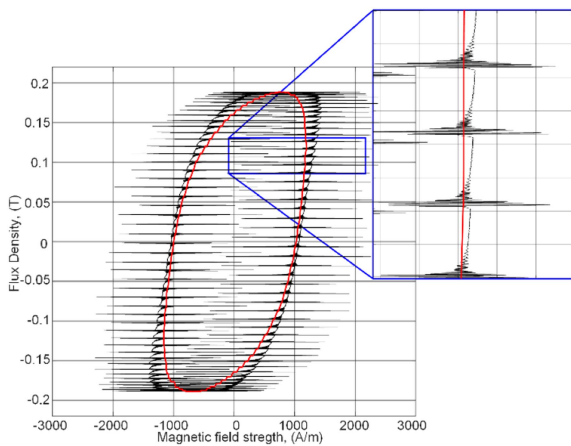


**FIGURE 5.** Dynamic hysteresis loops for sample #1 at fundamental frequency = 2000 Hz, switching frequency = 100 kHz, and  $m_i = 0.9$ . In black: full spectrum signals; in red: fundamental flux density and magnetic field strength by the magnetizing current reconstructed using its first 50 harmonics.

dynamic hysteresis loops is representative of the extra losses introduced by the PWM switching [6], [7].

It is worth noting that the PWM voltage waveforms are similar to those obtained with a three-phase inverter, with marginal differences in terms of iron losses due to the different shifts in the modulations of the converter legs:  $120^\circ$  for the three-phase inverter instead of  $180^\circ$  for the H-bridge—refer to Appendix I.

**TABLE 5.** Technical Specifications of SiC MOSFETs

<i>SCTW100N120G2AG</i>	
Drain-source voltage	1200 V
Drain current (continuous) at $TC = 25^\circ C$	75 A
Max. switching frequency (@40% $I_{max}$ )	350 kHz
Drain-source on-resistance $R_{dson}$	30 m $\Omega$

The SiC H-bridge receives PWM command signals generated by the control board through an optical fiber interface. It then imposes the supply voltage  $v(t)$  at the sample primary winding. Specifications of SiC devices are given in Table 5. A fan is also utilized to maintain core temperatures below critical values. The waveforms of the primary current  $i(t)$  and the induced voltage in the sensing winding  $e(t)$  are acquired by an eight channels, 12-bit resolution oscilloscope (LeCroy MDA810A) using a 30 A, 50 MHz current probe (LeCroy CP030), and a 1.5 kV, 120 MHz high-voltage differential probe (LeCroy HVD3106), respectively. No digital filters have been activated for the voltage and current channels, and probe offsets were compensated both before each test and during the data processing. For each sample and each fundamental frequency value, preliminary tests were conducted by selecting the proper bus voltage value that maximizes the fundamental flux density in the core with a modulation index  $m_i = 1$ . Then, the flux density amplitude is regulated reducing  $m_i$  in steps of 0.1 until it reaches 0.2. For a selected sample and fundamental frequency value, the selected bus voltage is kept constant as the switching frequency changes.

For the accurate computation of the active power, the sampling frequency was properly set to obtain five MSamples in the measurement window, independently of the fundamental frequency value (e.g., 500 MS/s and a 10 ms measurement window for 2000 Hz). Consequently, harmonic components up to approximately 3 MHz are measured with very limited phase shifts [6], [19]. Furthermore, to compensate the unavoidable fluctuations in power measurements under the PWM supply, each measurement point was acquired three times. A time-consuming data processing step in MATLAB follows the measurements to compute the average rectified and root-mean-square values of the induced secondary voltage directly from the acquired samples. This is necessary for the estimation models that will be presented in Sections V and VI. Furthermore, a Fourier analysis of the waveforms has been implemented to compute the fundamental component of the flux density in the specimen and the corresponding fundamental specific iron losses. Note that the comprehensive characterization of a magnetic core sample requires approximately 15 h of measurements and data processing, requiring 40 GB of disk capacity to store the data. For measurements under “pure” sinusoidal supply, necessary to separate the hysteresis and eddy current loss components for use in loss estimations, an 18 kVA programmable pacific power source 360-AMX was used. This ac power source enables regulations from 0 to 340 V and 20–5000 Hz, with full power bandwidth

and an average total harmonic distortion of the output voltage lower than 0.25%. The adopted ac power source ensures a form factor in the sinusoidal induced voltage close to 1.11, also in saturated conditions.

To prevent any misunderstanding during the reading, in the following, the adjective “*fundamental*” will refer to the lowest order harmonic in a distorted periodic waveform (e.g., the blue signal shown in Fig. 4). The frequency of the lowest order harmonic will be referred to as the fundamental frequency  $f_{fund}$ . The adjective “*sinusoidal*” refers to the electric quantities measured supplying the load with an ac sinusoidal source. As a sinusoidal signal has no higher order harmonics, it is correct to call its frequency still fundamental frequency. Finally, the adjective “*full spectrum*” refers to the computation of electrical quantities considering their overall harmonic content in the frequency range of the instrument.

**IV. INITIAL EXPERIMENTAL INVESTIGATIONS AT LOW FUNDAMENTAL FREQUENCIES**

At the fundamental frequency of 50 Hz, sample #1 was tested for all the deadtime/switching frequency combinations, as shown in the matrix of Fig. 1, while for the fundamental frequency of 200 Hz, the lowest switching frequency used in the tests was limited to 10 kHz. The following four experimental test campaigns have been initially carried out.

- 1) Sample #1 tested at  $f_{fund} = 50$  Hz and  $B_{max} = 1.6$  T: deadtime = 150–300–450 ns,  $f_{sw} = 1$ –200 kHz, see Fig. 6.
- 2) Sample #1 tested at  $f_{fund} = 200$  Hz and  $B_{max} = 1.6$  T: deadtime = 150–300–450 ns,  $f_{sw} = 10$ –200 kHz, see Fig. 7.
- 3) Sample #2 tested at  $f_{fund} = 50$  Hz and  $B_{max} = 2.2$  T: deadtime = 150–300–450 ns,  $f_{sw} = 1$ –200 kHz, see Fig. 8.
- 4) Sample #2 tested at  $f_{fund} = 200$  Hz and  $B_{max} = 2.2$  T: deadtime = 150–300–450 ns,  $f_{sw} = 10$ –200 kHz, see Fig. 9.

Figs. 6 and 7 provide detailed insights into the impact of the switching frequency on the specific iron losses for the two considered cores. In particular, the iron losses monotonically decrease as the switching frequency increases. These findings are consistent with those presented in [6] and [11], but differ from those reported in [7], where the iron losses at  $B_{max} = 1.0$  T initially decrease, but they rise again above 100 kHz.

In the explored flux density range, for the sample #1, the iron losses for switching frequencies above 100 kHz have been found to be practically constant and slightly larger than the ac iron losses, at both 50 and 200 Hz—see Figs. 6 and 7. The same general conclusion can be drawn also for the cobalt-iron material, as shown in Figs. 8 and 9. Taking care that the scales of the vertical axes are different, a comparison between Figs. 6(b) and 8(b), as well as Figs. 7(b) and 9(b), reveals that the loss increase from the ac and PWM trends is roughly the same for the two samples across the entire switching frequency range. Consequently, the percentage loss increase

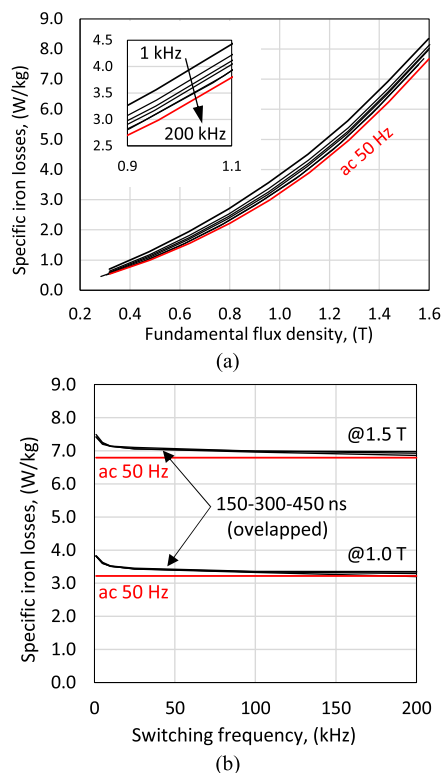


**FIGURE 6.** Switching frequency impact on the iron losses for the sample #1 at 50 Hz: (a) 150 ns and (b) 150, 300, and 450 ns deadtimes.

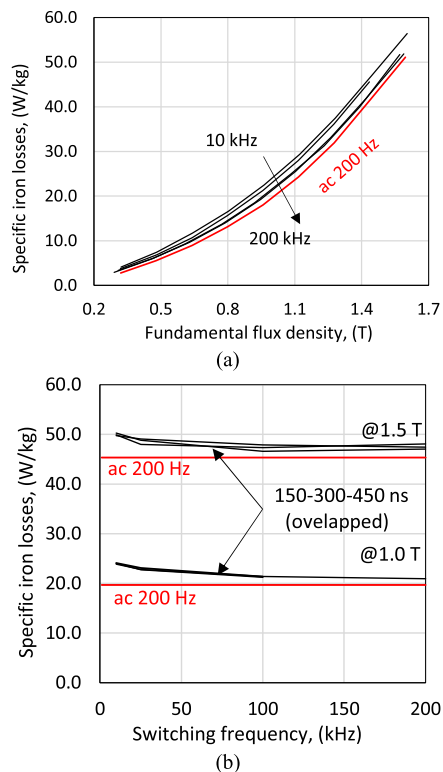


**FIGURE 7.** Switching frequency impact on the iron losses for the sample #1 at 200 Hz: (a) 150 ns and (b) 150, 300, and 450 ns deadtimes.

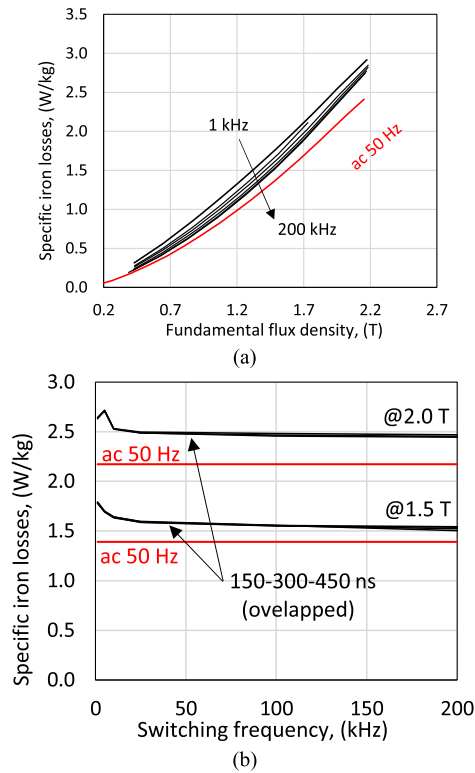


**FIGURE 8.** Switching frequency impact on the iron losses for the sample #2 at 50 Hz: (a) 150 ns and (b) 150, 300, and 450 ns deadtimes.

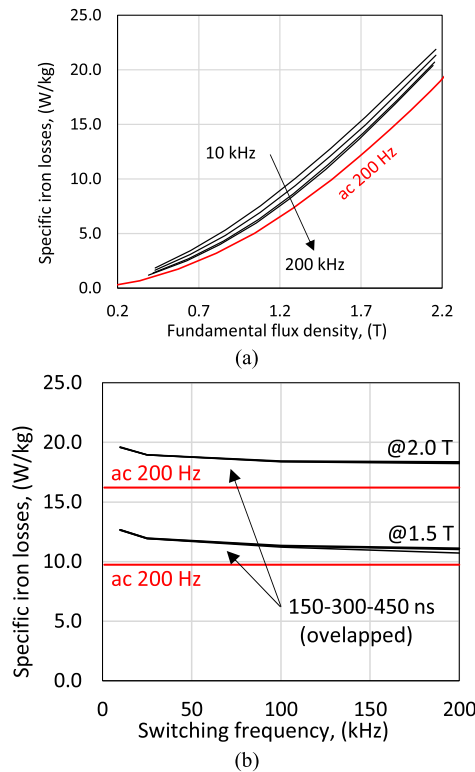


**FIGURE 9.** Switching frequency impact on the iron losses for the sample #2 at 200 Hz: (a) 150 ns and (b) 150, 300, and 450 ns deadtimes.

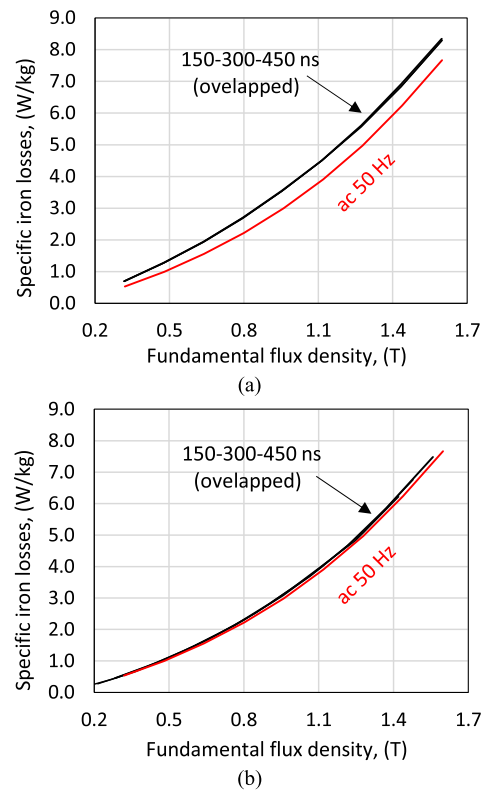


**FIGURE 10.** Deadtime effects on the iron losses of the sample #1 at  $f_{\text{fund}} = 50$  Hz for (a)  $f_{\text{sw}} = 1$  kHz and (b)  $f_{\text{sw}} = 200$  kHz switching frequencies.

due to the PWM switching is larger in the 0.35 mm FeCo material instead of the 0.5 mm FeSi one. As clearly proven by Figs. 10 and 11, the test results do not highlight any significant dependence of the specific losses on the deadtime, as all three black trends perfectly overlap. In this case, this finding aligns well with the observations reported in [7], although a different magnetic material, geometrical dimensions of the toroid, fundamental frequency, and WBG technology were used.

## V. IRON LOSS MODELING UNDER HIGH SWITCHING FREQUENCIES PWM SUPPLY

The prediction of iron losses under arbitrarily distorted waveform is a challenge, especially when the excitation is a high switching frequency PWM waveform. Models of iron loss estimation have been widely investigated and can be categorized into two main classes: practical methods for fast but reasonably accurate loss quantification; and sophisticated estimated models capable of considering all the complex phenomena in the presence of highly distorted waveforms (e.g., the core loss increases due to minor loops in the hysteresis fundamental cycle). While the former category is typically developed starting from experiments and data fitting of the measurements, the latter is usually developed using finite-element methods (FEMs) software. A valuable example of

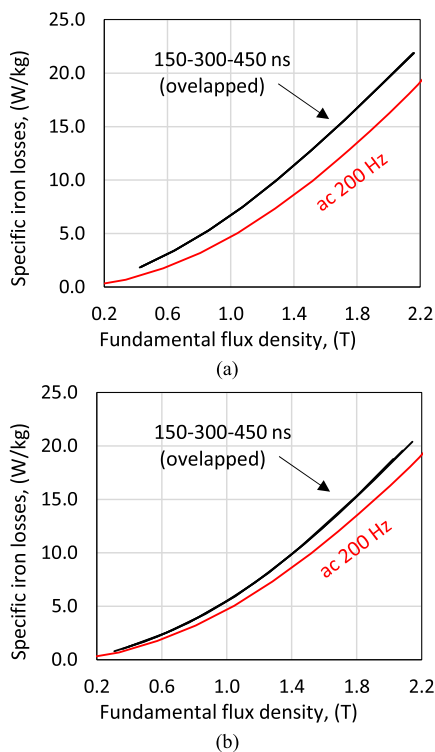


**FIGURE 11.** Deadtime effects on the iron losses of the sample #2 at  $f_{\text{fund}} = 200$  Hz for (a)  $f_{\text{sw}} = 10$  kHz and (b)  $f_{\text{sw}} = 200$  kHz switching frequencies.

an estimation method belonging to the second category is presented in [11] and [12].

Even if the results provided in these articles can be considered accurate, the method is challenging to implement during the initial design stage of high-speed electrical machines. At this stage, the machine geometry is continuously refined, and the PWM characteristics are far from being selected. Additionally, the model parameters have to be determined through ac loss measurements at very high frequency and very low flux density values with an overlapped dc bias. These measurements typically require “*ad hoc*” specimens and test rigs, not stator magnetic cores.

At the moment, it is not clear how to generalize the material coefficients presented in [12] to other thin high-grade magnetic laminations, perhaps of a different alloy. Even neglecting the time to perform the FEM simulations, the user must be an expert in magnetic measurements and must have excellent skills in data processing and software usage.

For the aforementioned reasons, the authors aim to develop a more “*user-friendly*” estimation method. As will be articulated in Section V-A and B, the starting point is the applicability check of a previously published methodology and its extension to operating switching frequencies of WBG-based PWM inverters.

### A. INITIAL IRON LOSSES MODELING

A straightforward analytical method was proposed in [16] and validated with the inverter technology available at the time. It

proved to be effective for switching frequencies ranging from 1 to 5 kHz and a deadtime ranging from a few to 10  $\mu\text{s}$ . Hereafter, the method is briefly outlined and initially applied using the measurements on the sample #1 and sample #2 during the low fundamental frequency test campaign, as presented in Section IV. The proposed approach assumes that, in the absence of minor hysteresis loops, the iron loss under PWM can be theoretically computed, knowing the hysteresis losses  $P_{\text{hysteresis}_{\text{sin}}}$  and eddy current losses  $P_{\text{eddy current}_{\text{sin}}}$  with sinusoidal supply at the same fundamental flux density by using (1). In this equation,  $\nu$  is the Steinmetz coefficient of magnetic material, while “avg” and “rms” indicate the average rectified value and the root-mean-square values of the induced voltage  $e(t)$  in the secondary winding, both for the fundamental component and full spectrum PWM-induced voltages

$$P_{\text{iron}_{\text{PWM}}} = \alpha^{\nu} P_{\text{hysteresis}_{\text{sin}}} + \beta^2 P_{\text{eddy current}_{\text{sin}}}$$

$$\alpha = \frac{E_{\text{avg,PWM}}}{E_{\text{avg,fundamental}}}, \quad \beta = \frac{E_{\text{rms,PWM}}}{E_{\text{rms,fundamental}}}. \quad (1)$$

In [16], the coefficients  $\alpha$  and  $\beta$  were introduced to account for the effects of distortion of the PWM waveform with respect to its fundamental component, in a sort of “equivalent” or “engineering” way. The coefficients  $\alpha$  and  $\beta$  to be used in (1) are computed from the measurements collected during the test campaign, as described in Section IV, and they are shown in Fig. 12. The red trends in these figures refer to the lowest switching frequency used in the tests and are practically identical to their theoretical values for an ideal unipolar sine-triangle PWM waveform, calculable using the equation reported in Appendix I for 180° of phase shift. Interestingly, the spread of  $\alpha$  and  $\beta$  values at 200 kHz is more evident at 50 Hz than at a fundamental frequency of 200 Hz. In any case, Fig. 12 summarizes well that, at a low modulation index, the actual PWM voltage is more distorted than the ideal PWM waveform

$$P_{\text{iron}_{\text{sin}}} = P_{\text{hysteresis}_{\text{sin}}} + P_{\text{eddy current}_{\text{sin}}}$$

$$P_{\text{hysteresis}_{\text{sin}}} = k_h \cdot f \cdot B^{\nu}; \quad P_{\text{eddy current}_{\text{sin}}} = k_{\text{ec}} \cdot f^2 \cdot B^2. \quad (2)$$

The main advantage of using model (1) is that the iron losses under PWM supply can be estimated from the knowledge of the above coefficients and the iron losses in the case of sinusoidal supply. However, the latter must be separated in their basic components in accordance with (2): the hysteresis losses and the “global” eddy currents (sum of the classical eddy current losses and Bertotti’s excess losses). By adopting (2) and performing measurements under ac sinusoidal supply at variable excitation frequency  $f$  and variable flux density amplitudes  $B_{\text{max}}$ , the hysteresis coefficients  $k_h$ ,  $\nu$ , and the eddy current coefficient  $k_{\text{ec}}$  can be easily determined. For example, this can be achieved by applying a least square fitting of the specific iron losses expressed in W/kg. In the present study, the loss separation under ac sinusoidal supply has been conducted in the range 20–200 Hz and 0.3–1.6 T for the Fe-Si toroidal core, while the cobalt–iron sample was tested at 50,

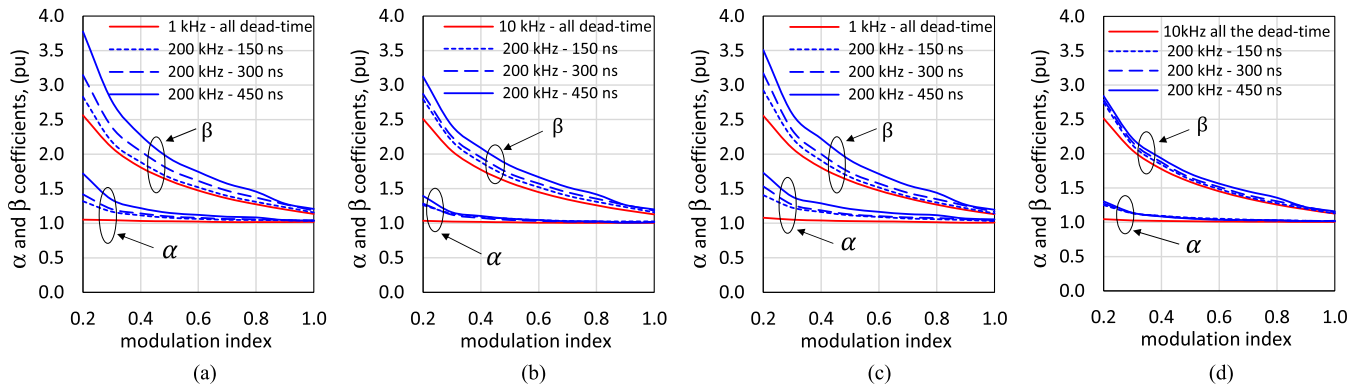


**FIGURE 12.** Measured  $\alpha$  and  $\beta$  coefficients versus modulation index and switching frequency. (a) Sample #1 @ 50 Hz. (b) Sample #1 @ 200 Hz. (c) Sample #2 @ 50 Hz. (d) Sample #2 @ 200 Hz.

**TABLE 6.** Material Coefficients for the Sinusoidal Loss Model (2) for the 50–200 Hz Frequency Range

Coefficient	Sample #1	Sample #2
$k_h$	0.0516	0.0115
$v$	1.716	1.451
$k_{ec}$	0.00026	0.000062

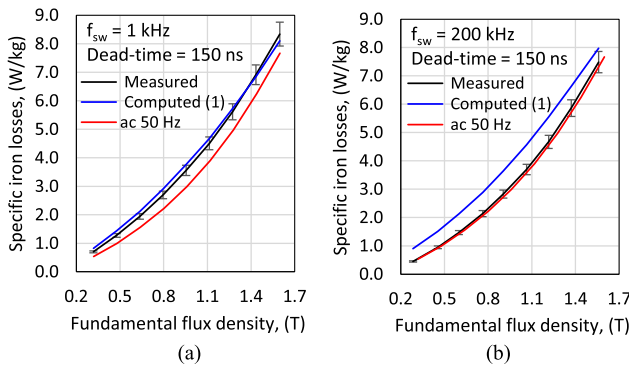


**FIGURE 13.** Iron loss prediction for sample #1 at the fundamental frequency of 50 Hz for switching frequencies equal to (a) 1 kHz and (b) 200 kHz.

100, and 200 Hz and 0.4–2.2 T. The material coefficients are reported in Table 6.

Based on the findings presented in Section VI, the model evaluation has been conducted only for the measurements executed with a deadtime equal to 150 ns. The coefficients  $\alpha$  and  $\beta$  have been used to predict iron losses under PWM supply by using (1).

Due to space limitations and considering that the comparative results are similar for all fundamental/switching frequency combinations, only selected results are reported. Figs. 13 and 14 show the specific iron losses of sample #1 and sample #2 for various values of the fundamental and switching frequencies.

In these figures, the error bars at  $\pm 5\%$  have been set for each measured iron loss curve. Looking at these figures and

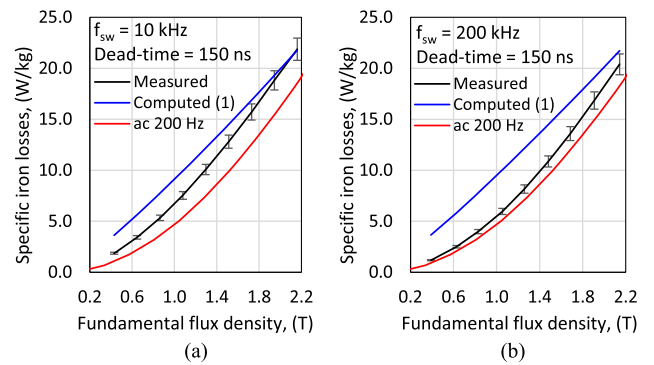


**FIGURE 14.** Iron loss prediction for sample #2 at the fundamental frequency of 200 Hz, for switching frequencies equal to (a) 10 kHz and (b) 200 kHz.

observing that  $P_{\text{hysteresis}_{\text{sin}}}$  and  $P_{\text{eddy current}_{\text{sin}}}$  are invariant with respect to the PWM characteristics, for a fixed fundamental flux density, it is possible to conclude that (1) can be reasonably used only for switching frequencies smaller than 5 kHz, approximately.

## B. REFINEMENT OF THE IRON LOSS MODEL

It should be remarked that method (1) is theoretically correct as long as there are no minor loops in the hysteresis cycle and the impact of the skin effect in the magnetic laminations is reasonably negligible, as in the fundamental frequency range of 50–200 Hz. However, the previous analysis shows that (1) cannot intrinsically predict the iron losses when a high switching frequency is used because  $\alpha$  and  $\beta$  are greater than or equal to one, and the specific iron losses decrease as the switching frequency increases. Nonetheless, by pursuing a modified formulation of (1) able to model the reduction of the eddy current loss contribution as the switching frequency increases, the authors propose to use the following equation:

$$P_{\text{iron}_{\text{PWM}}} = \alpha^v P_{\text{hysteresis}_{\text{sin}}} + k(f_{\text{fund}}, f_{\text{sw}}, B_{\text{fund}}) \cdot \beta^2 P_{\text{eddy current}_{\text{sin}}}. \quad (3)$$



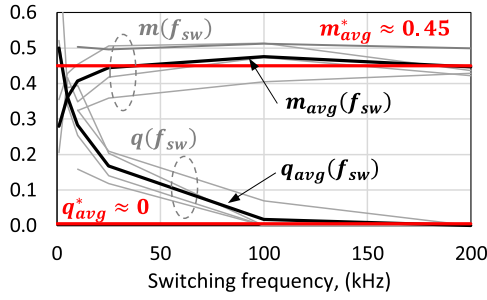


**FIGURE 15.**  $m(f_{sw})$  and  $q(f_{sw})$  parameters for the use of (4). The four gray trends are the identified values at 50 and 200 Hz for the sample #1 and sample #2, while the black trends are the average of the gray ones.

In this new estimation model, the loss contribution coming from  $P_{\text{hysteresis, sin}}$  has not been changed because  $\alpha$  is close to one at high flux density values or, equivalently, at high modulation indices. A corrective term  $k(f_{\text{fund}}, f_{\text{sw}}, B_{\text{fund}})$  is included in the expression of (3) to nullify the differences between estimates and measurements. Initially, the unknown coefficient  $k$  has been numerically determined by applying the least square fitting procedure, both at the 50 and 200 Hz measurements. For each switching frequency value, a linear trend of unknown  $k$  versus the flux density has been observed. Consequently, the authors propose the following relation for the coefficient  $k$ :

$$k(f_{\text{fund}}, f_{\text{sw}}, B_{\text{fund}}) = m(f_{\text{fund}}, f_{\text{sw}}) B_{\text{fund}} + q(f_{\text{fund}}, f_{\text{sw}}). \quad (4)$$

Once again, least squares fitting has been applied to the measured values, but this time considering the constraint (4). During the data processing of the measurements at 50 and 200 Hz, it has been observed that  $m(f_{\text{fund}}, f_{\text{sw}}) \approx m(f_{\text{sw}})$  and  $q(f_{\text{fund}}, f_{\text{sw}}) \approx q(f_{\text{sw}})$ . Moreover, Fig. 15 shows that the four gray curves estimated for the sample #1 and sample #2 at 50 and 200 Hz have similar trends and are close to each other.

The latter observation leads to the possibility to define the average black trend  $m_{\text{avg}}(f_{\text{sw}})$  and  $q_{\text{avg}}(f_{\text{sw}})$  that can be used in the model (3) in substitution of the specific gray trends, obtaining in this way the so-called model “(3)-avg.” A further simplification in (4) can be introduced by observing that, in Fig. 15,  $m(f_{\text{sw}}) \approx 0.4\text{--}0.5$  for switching frequency in the 10–200 kHz range and  $q(f_{\text{sw}}) \approx 0$  above the 100 kHz, independently of the magnetic material grade and fundamental frequency. Hence, the idea of considering two constant coefficients  $m_{\text{avg}}^*$  and  $q_{\text{avg}}^*$  in (4), regardless of the core sample and the switching frequency value used. This assumption allows defining the further model “(3)-avg\*.” In other words, the model can be formed in a number of ways according to the complexity level for the identification of the parameters of (4) and the desired accuracy in the estimations.

- 1) Model (3) adopts the  $m(f_{\text{sw}})$  and  $q(f_{\text{sw}})$  by definition.
- 2) Model “(3)-avg” uses the  $m_{\text{avg}}(f_{\text{sw}})$  and  $q_{\text{avg}}(f_{\text{sw}})$  trends.

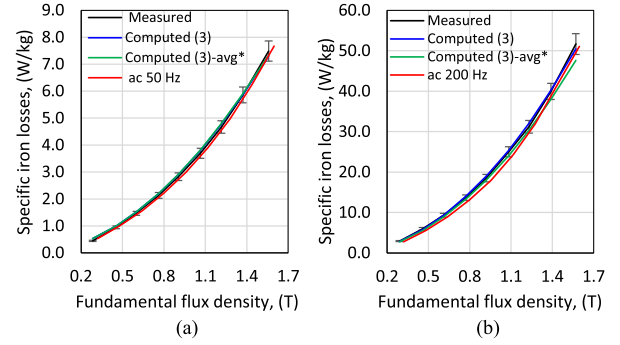


**FIGURE 16.** Iron loss prediction for the sample #1 for a switching frequency of 200 kHz. (a)  $f_{\text{fund}} = 50$  Hz. (b)  $f_{\text{fund}} = 200$  Hz.

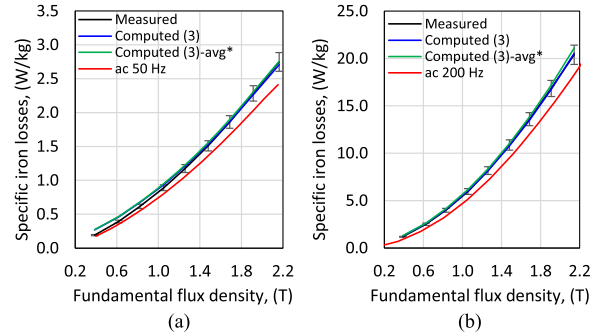


**FIGURE 17.** Iron loss prediction for the sample #2 for a switching frequency of 200 kHz. (a)  $f_{\text{fund}} = 50$  Hz. (b)  $f_{\text{fund}} = 200$  Hz.

- 3) Model “(3)-avg\*” uses the constant values  $m_{\text{avg}}^*$  and  $q_{\text{avg}}^*$ .

Figs. 16 and 17 show the results obtained by implementing the proposed modeling methods for the sample #1 and the sample #2 supplied by PWM voltages at  $f_{\text{sw}} = 200$  kHz and  $f_{\text{fund}} = 50$  Hz and 200 Hz. It has been considered only the maximum switching frequency as it represents the worst case for the original estimation model (1). As the results of the model “(3)-avg” are practically identical to those by the model (3), the former has not been included in the figures for better readability. Looking at the Figs. 16 and 17, it is evident that the linear approximation (4) of  $k(f_{\text{fund}}, f_{\text{sw}}, B_{\text{fund}})$  allows achieving a perfect match between the measured and the computed specific iron losses when the specific trends  $m(f_{\text{sw}})$  and  $q(f_{\text{sw}})$  are used; in fact, as expected, the black and blue curves are perfectly overlapped. This happens for all the fundamental and switching frequency values explored in the initial test campaign. The green trends in Figs. 16 and 17 represent the loss estimations based on model “(3)-avg\*.” They are unquestionably accurate, confirming that the assumption of  $m_{\text{avg}}^* = 0.45$  and  $q_{\text{avg}}^* = 0$  also below 100 kHz is definitively acceptable, at least at the low fundamental frequencies. Note that the possibility of using constant values  $m_{\text{avg}}^*$  and  $q_{\text{avg}}^*$  for any switching frequencies is extremely intriguing considering that the sample #1 and the sample #2 feature very different characteristics in terms of magnetic material quality,

**TABLE 7. Summary of the Tests Performed on the Four Samples**

$f_{sw}$ , (kHz)	Fundamental frequency, (Hz)				
	400	800	1000	1500	2000
50	all	#1, #2	all	all	all
100	all	#1, #2	all	all	all
150	#3, #4	none	#3, #4	#3, #4	#3, #4
200	all	#1, #2	all	all	all
350	all	#1, #2	all	all	all

**TABLE 8. Material Coefficients for the Sinusoidal Loss Model (2) at Different Fundamental Frequency Ranges**

	$f_{fund}$ range, (Hz)	$k_h$	$v$	$k_{ec}$
Sample #1	50-200	0.0477	1.716	$27.8 \cdot 10^{-5}$
	400-800	0.0859	1.758	$11.0 \cdot 10^{-5}$
	1000-2000	0.0862	1.758	$10.6 \cdot 10^{-5}$
Sample #2	50-200	0.0118	1.451	$7.09 \cdot 10^{-5}$
	400-800	0.0207	1.969	$3.70 \cdot 10^{-5}$
	1000-2000	0.0253	1.775	$2.75 \cdot 10^{-5}$
Sample #3	50-200	0.0200	1.728	$6.56 \cdot 10^{-5}$
	400-2000	0.0274	1.747	$4.49 \cdot 10^{-5}$
Sample #4	50-200	0.0205	1.725	$6.96 \cdot 10^{-5}$
	300-500	0.0202	1.616	$6.52 \cdot 10^{-5}$
	1000-2000	0.0397	1.657	$4.75 \cdot 10^{-5}$

thickness, saturation levels, and so on. Unfortunately, as will be discussed in Sections VI and VII, this is not enough to generalize the finding for any type of magnetic laminations and high fundamental frequencies.

## VI. IRON LOSS MEASUREMENTS AND MODELING AT HIGH FUNDAMENTAL FREQUENCIES

The four samples, as presented in Tables 1–4, have also been tested under PWM voltages synthesizing fundamental harmonics of 400–2000 Hz and switching frequencies ranging from 50 to 350 kHz. Based on the previous experiences, all the tests were conducted with a deadtime equal to 150 ns. The high-frequency tests are summarized in Table 7. The term “all” means that all four specimens have been tested at the specified frequencies. To extend the application of model (3) to high frequencies, it is essential to understand how to separate the hysteresis and eddy current losses in a wide frequency range of the ac sinusoidal supply. For the high-frequency test campaign, samples #3 and #4 were characterized by direct testing under sinusoidal excitation, while samples #1 and #2 were studied considering the fundamental iron losses measured with PWM voltage. This is the reason for the slight differences in values reported in the 50–200 Hz frequency range between Tables 6 and 8.

However, these negligible differences further demonstrate that, in cases where the ac sinusoidal characterization of the magnetic material is unavailable, the fundamental power measured under PWM could be employed as a substitute of the iron losses measured with sinusoidal supply [20]. The identification of the coefficients  $k_h$ ,  $v$ , and  $k_{ec}$  in (2) is performed by conducting a curve fitting based on the least square method approximation, and the results are listed in Table 8.

The estimation accuracy of model (3) is highly sensitive to the Steinmetz exponent  $v$  and, consequently, to the ratio  $P_{hysteresis, sin} / P_{eddy, current, sin}$ . Thus, it is suggested to proceed with the unknowns’ identification using limited frequency ranges [14], [21]. From the practical point of view, the ranges, as reported in Table 8, have been determined by searching an excellent data fitting in the widest possible frequency range. Additionally, it is of paramount importance to have the estimated coefficients  $k_h$ ,  $v$ , and  $k_{ec}$  under sinusoidal supply at the same PWM fundamental frequencies. In this way, the impact of the skin effect due to a fundamental frequency increase under PWM supply is “automatically” accounted using the proper set of the coefficients  $k_h$ ,  $v$ , and  $k_{ec}$ .

Due to the space limitation, only the estimated iron losses for the minimum and maximum values of the fundamental and switching frequencies (highlighted in green in Table 7) are reported in Table 9 for each sample. The estimated losses from model (3) were computed using the measured coefficients  $\alpha$  and  $\beta$ , as shown in Table 10. Similar to the observations in the low fundamental frequency range, the results of Table 9 underline that, with the increase of the switching frequency, the measured losses shift toward the ac or fundamental trends. However, while at 400 Hz, the full-spectrum measured iron loss trends at 50 and 350 kHz are very close to the corresponding ac red curves, they are further apart for the cases of fundamental frequency equal to 2000 Hz. This result confirms once again the need to have a straightforward model suitable to predict the extra iron losses introduced by the PWM inverter, especially at high fundamental and switching frequency. From the loss estimation accuracy viewpoint, the dashed blue trends in Table 9 show that, also at high frequency, the model (1) is not able to accurately predict the specific losses for the same reason, as explained in Section V, while the model (3) provides excellent results, in particular for the sample #1 and sample #2.

It should be noted that the loss estimate (3) for the sample #3 and the sample #4 worsens compared with the other two cores, with the exception of the sample #3 tested at 50 kHz. In particular, even if the  $m(f_{fund}, f_{sw})$  and the  $q(f_{fund}, f_{sw})$  have been again identified for each  $(f_{fund}, f_{sw})$  combination in the high frequency ranges, the curves of the model (3) fit the measurements in the  $\pm 5\%$  error bars only for modulation index between 0.5 and 1, approximately. In these cases, for the sample #3 and sample #4, there is a crossing between the measured (black) and computed (3) trends (i.e., the continuous blue curves), approximately for a modulation index equal to 0.8. The difference in the “bending” of the black and blue trends is attributable to the used least squares fitting that does not converge properly for the lowest values of the modulation index.

Being the loss segregation in sinusoidal supply independent of the measurements under PWM supply, the problem is reasonably due to an unexpected spread of the coefficients  $\alpha$  and  $\beta$  measured at low modulation index.

Table 10 lists the curves of the measured coefficients  $\alpha$  and  $\beta$  at 50 (in black) and 350 kHz (in blue) together with their

**TABLE 9. Measurement and Computed Specific Iron Losses for Selected Cases (Green Cells in Table 7)**

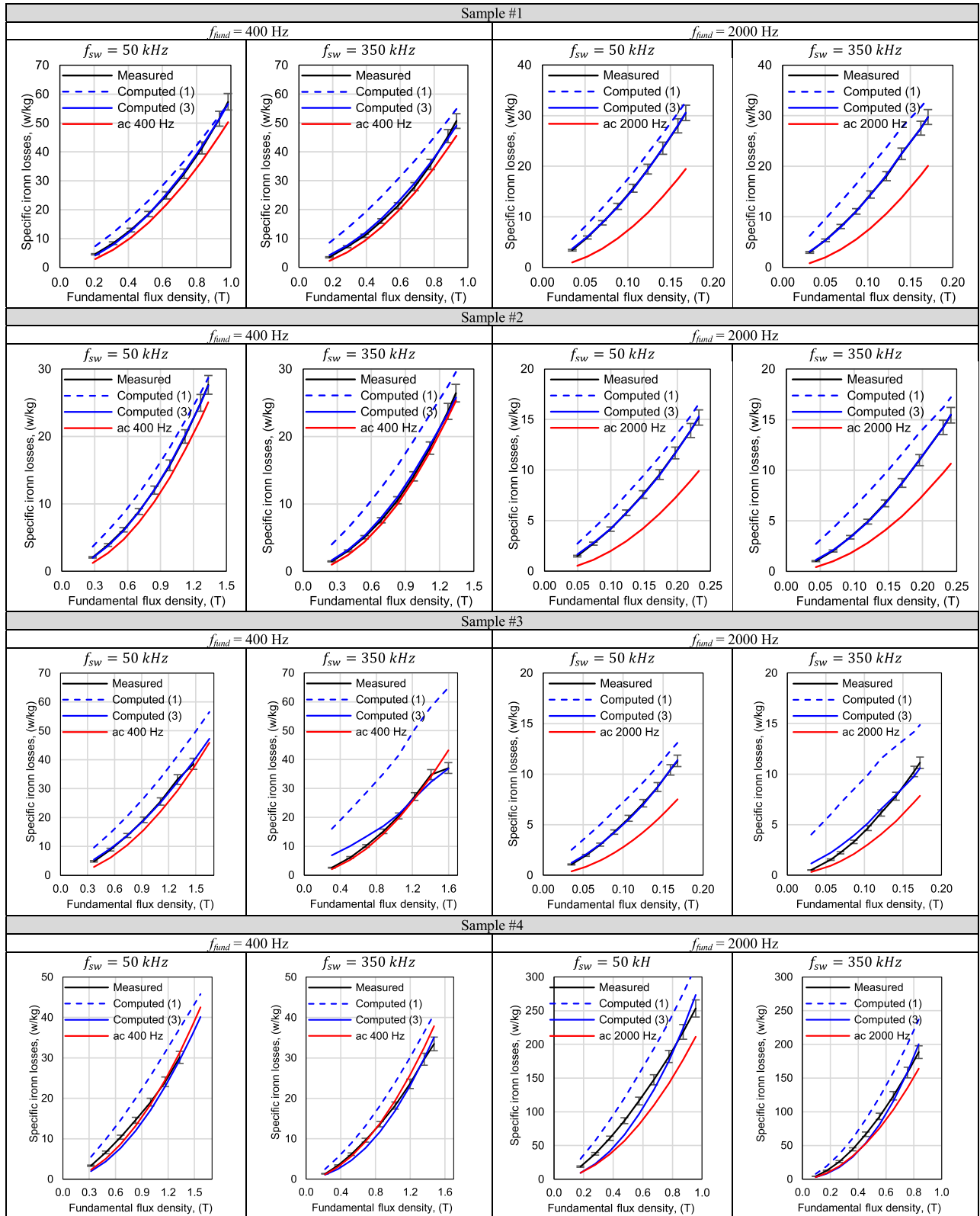
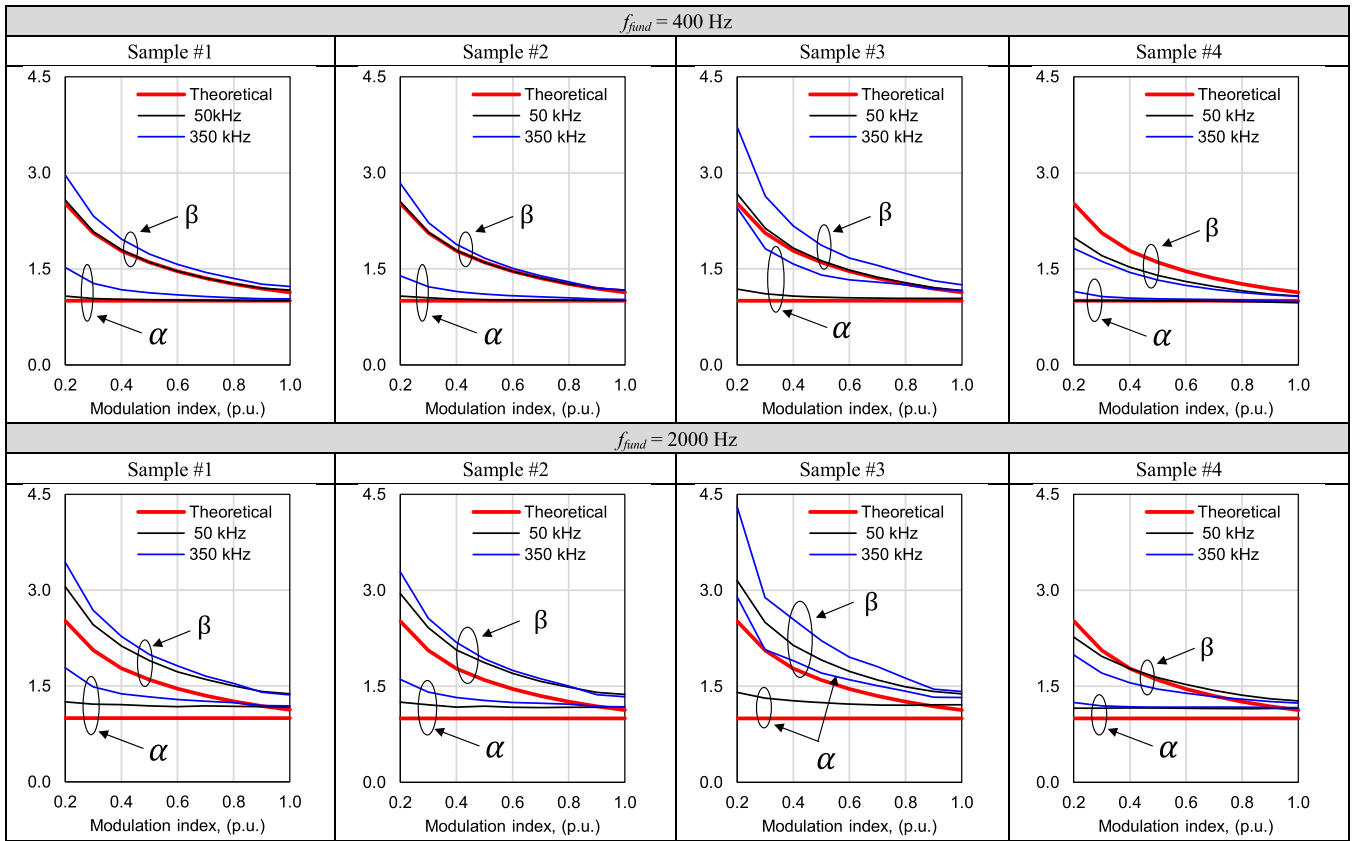


TABLE 10.  $\alpha$  and  $\beta$  Coefficients for Selected Cases (Green Cells in Table 7)



theoretical values (in red). For the assumed ideal unipolar sine-triangle PWM waveform with  $180^\circ$  shift modulation, the expression of the coefficients  $\alpha$  and  $\beta$  can be found in Appendix I. At 400 Hz and 50 kHz, the sample #1 and sample #2 measured values are practically equal to the theoretical ones, while with the increase of both the switching and fundamental frequency, the measured values increase in a “regular” way. In Table 10, an anomalous increase in the coefficient  $\beta$  is noticeable at the highest switching frequency for sample #3. Meanwhile, the coefficient  $\beta$  for sample #4 is even lower than its theoretical value. It is possible to conclude that these two anomalous behaviors observed for the sample #3 and sample #4 reflect bigger estimation errors.

These trends can be attributed to resonance phenomena or very low inductance values (i.e., high current ripples). These assumptions are corroborated by measurements of the primary winding impedance of the samples under test, conducted using a precision LCR meter. The results are reported in Figs. 20 and 21 of Appendix II. In the case of sample #3, the amplitude–frequency response is comparable with those of sample #1 and sample #2, but a resonance at approximately 380 kHz is evident, which is very close to the maximum switching frequency used in the tests. Conversely, sample #4 exhibits a very small inductance value due to its big yoke cross section and low turn numbers. Abnormal distortions of PWM voltages are observed in both cases and oscilloscope

measurements of the coefficients  $\alpha$  and  $\beta$  cannot be considered reliable.

In the authors’ opinion, when there are resonances or severe ripples in the primary current, the oscilloscope measurements of the full spectrum powers and the fundamental component of the voltages and current can still be considered reliable. This is because the full spectrum electrical power is directly computed from the acquired waveform samples, applying the active power definition. On the other hand, in the mentioned anomalous conditions for the sample #3 and sample #4, it has been experimentally verified that the fundamental active power cannot be considered likewise consistent, as it is derived from the math implemented in the data postprocessing. This is probably due to anomalous changes of the phase shift between the voltage and current fundamental harmonics for unquestionable triggering issues under PWM supply at a very high switching frequency.

The previous analysis shows that, under anomalous operating conditions, the measured coefficients  $\alpha$  and  $\beta$  can introduce larger loss estimation errors with respect to those computed under regular conditions because they depend not only on the characteristic of the PWM (e.g., deadtime, rise time, etc.) but also on the sample dimensions and in what manner the specimen has been wound.

Even though under anomalous operating conditions, the measured coefficients  $\alpha$  and  $\beta$  can introduce larger loss

**TABLE 11. Average Percentage Errors in Loss Estimation Using the Model (3)—Error = 100\*(Computed-Measured)/Measured**

$f_{sw}$ , (kHz)	Fundamental frequency, (Hz)				
	400	800	1000	1500	2000
Sample #1					
50	0.5	0.0	-0.1	-0.3	-0.3
100	0.6	0.0	-0.1	-0.3	-0.3
200	1.1	0.0	-0.1	-0.3	-0.1
350	2.3	0.1	0.1	0.1	0.0
Sample #2					
50	0.2	-0.1	-0.1	-0.4	-0.3
100	0.4	0.0	0.0	-0.4	-0.5
200	0.5	0.0	-0.1	-0.4	-0.4
350	2.0	-0.1	-0.3	-0.5	-0.3
Sample #3					
50	3.3	n.a.	-0.5	-0.6	-0.7
100	3.4	n.a.	-0.7	-0.7	-0.7
150	2.8	n.a.	0.0	-0.4	-0.5
200	2.0	n.a.	1.2	1.0	0.7
350	1.2	n.a.	5.9	5.2	4.6
Sample #4					
50	-4.5	n.a.	-5.3	-6.5	-7.3
100	-4.3	n.a.	-5.4	-6.7	-7.8
150	-5.6	n.a.	-5.6	-7.1	-8.0
200	-5.7	n.a.	-5.8	-7.5	-8.6
350	-6.3	n.a.	-6.3	-8.5	-9.5

**TABLE 12. Average Percentage Errors in Loss Estimation Using the Practical Model “(3)-Avg”—Error = 100\*(Computed-Measured)/Measured**

$f_{sw}$ , (kHz)	Fundamental frequency, (Hz)				
	400	800	1000	1500	2000
Sample #1					
50	-0.3	-1.0	-2.1	-1.2	-2.4
100	0.4	1.3	1.2	0.0	-0.5
200	2.6	1.6	1.3	1.5	0.6
350	1.2	-0.6	0.6	-0.1	2.2
Sample #2					
50	-4.1	-2.7	-2.7	-3.6	-3.9
100	0.9	0.0	-0.2	-0.2	-0.6
200	2.3	1.6	1.5	0.9	1.6
350	3.7	2.0	1.9	2.1	2.8
Sample #3					
50	-4.9	n.a.	-4.8	-5.6	-5.1
100	-1.4	n.a.	-2.0	-1.6	-2.0
150	0.5	n.a.	0.1	0.0	-0.4
200	2.4	n.a.	1.3	1.6	0.8
350	4.3	n.a.	4.6	5.1	5.5
Sample #4					
50	-1.8	n.a.	-2.3	-1.2	-3.8
100	3.0	n.a.	0.5	1.3	1.4
150	1.4	n.a.	1.3	3.7	3.6
200	1.3	n.a.	1.2	2.3	0.4
350	-1.8	n.a.	-1.0	-0.7	-2.6

estimation errors, in terms of average errors; model (3) provides very good estimations of the losses in the high-frequency ranges for all the tested samples—see Table 11.

The average errors have been computed using the loss estimates for modulation index greater than 0.5. In the table, errors lower than 5% are highlighted in green, while those in the 5–15% range are highlighted in yellow. Note that also for the sample #3 and sample #4, the results can be considered much more than satisfactory, also considering that, for

modulation index around 0.8, the agreement between measurements and estimations is excellent—see Table 9.

**VII. DESIGN-ORIENTED IRON LOSS MODEL**

While model (3) can be effectively utilized to determine the accurate analytical estimation of iron losses, it requires data fittings applied to sophisticated test measurements. From this viewpoint, model (3) can be usefully adopted to characterize different types of magnetic materials for research purposes. However, this does not prevent the same model from also being used at a design level of an electrical machine to predict the extra core losses due to the WBG-based inverter excitation. In the following text, practical insights are provided on the modified version of model “(3)-avg” developed for being used to predict iron losses at high fundamental frequencies, along with guidelines on its application and a critical discussion about the limits of this approach.

**A. DESIGN-ORIENTED VERSION OF MODEL “(3)-AVG” FOR HIGH FUNDAMENTAL FREQUENCIES**

The design-oriented version of model “(3)-avg” is determined by computing the coefficients  $\alpha$  and  $\beta$  associated with each sample according to ideal PWM voltages, thus using a set of  $m$  and  $q$  that only depend on  $f_{fund}$ .

In this way, the data-fitting procedure is less affected by the specific test conditions. Contrary to what was observed during the low fundamental frequency tests, a very good fitting of the high fundamental frequency measurements can be obtained by expressing the average parameters in (4) as a function of the  $f_{fund}$  only. In other words, model “(3)-avg” makes use of the coefficients  $m_{avg}(f_{fund})$  and the  $q_{avg}(f_{fund})$  for all the considered switching frequencies. For the four tested samples, the  $m_{avg}(f_{fund})$  and  $q_{avg}(f_{fund})$  trends are shown in Fig. 18, together with the average trends of the four tested samples, given by  $m_{avg}^*(f_{fund})$  and  $q_{avg}^*(f_{fund})$ . Their numerical values are reported at Appendix III from Tables 13 to 15.

The use of this modified version of model “(3)-avg” based on the coefficients  $m_{avg}(f_{fund})$  and  $q_{avg}(f_{fund})$  results in low-loss estimation errors. In fact, for all the samples, the errors are lower or very close to 5%, as shown in Table 12. This demonstrates the possibility to avoid measuring the coefficients  $\alpha$  and  $\beta$ , and confirms a negligible dependence of the average coefficients  $m$  and  $q$  by the switching frequency.

Unfortunately, the exciting idea of approximating the average coefficients  $m$  and  $q$  with constant values independent on the fundamental frequency, theorized during the low fundamental frequency tests—see Section V-B—is definitively over in the high-frequency ranges after having seen the trends of Fig. 18. This figure clearly shows that each sample has an own specific trend and that the use of the average coefficients  $m_{avg}^*(f_{fund})$  and  $q_{avg}^*(f_{fund})$  results in unacceptable estimation errors if the samples’ curves are “far” from the avg\* trends—see Table 16 in Appendix III—where the estimation errors are always lower than 20%, with the exception of the sample #4.

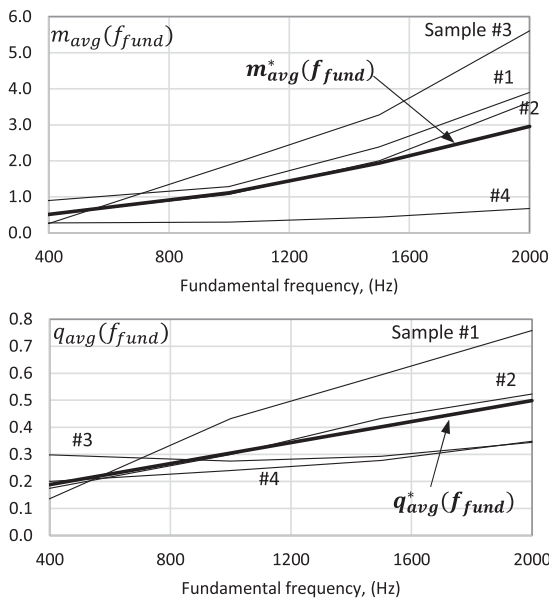


**FIGURE 18.**  $m_{avg}(f_{fund})$  and  $q_{avg}(f_{fund})$  parameters for the use of (4) at high fundamental frequency: the black avg\* curves are the average values for the four samples.

### B. STEP-BY-STEP PROCEDURE FOR THE USE OF MODEL “(3)-AVG”

The following procedure is proposed for the implementation of the practical use of the model “(3)-avg” at the early design stage of any ac electrical motor.

- 1) Select the magnetic material.
- 2) Segregate the iron losses under sinusoidal supply in the hysteresis and eddy current contributions using measurements or catalog data if the tests cannot be performed. At this step, it is possible to increase the specific losses reported in the datasheet with suitable building factors in order to take into account the magnetic material worsening due to the punching, stacking, and pressing of the core [22]. It is recommended to determine the unknown coefficients  $k_h$ ,  $v$ , and  $k_{ec}$  in the low-, medium-, and high-frequency ranges.
- 3) Estimate the modulation index for the selected flux density value and compute the theoretical coefficients  $\alpha$  and  $\beta$ . Remember that the maximum flux density should be obtained with a modulation index  $m_i = 1$ .
- 4) Select the coefficients  $m_{avg}(f_{fund})$  and the  $q_{avg}(f_{fund})$  by Fig. 18 or Tables 13–15. This is the most critical step because the “real” trends for the material selected at step 1 are unknown. Alternatively, as the first attempt, it is suggested to use the  $m_{avg}^*(f_{fund})$  and  $q_{avg}^*(f_{fund})$  values, being conscious that this can result in an 15%–20% loss underestimation for magnetic materials comparable to the one used for the sample #1 or in a very big loss overestimation as for the sample #4—see Table 16.
- 5) Predict the specific iron losses for high-frequency ranges using the model “(3)-avg.”

### C. CRITICAL DISCUSSION

First, the above arguments demonstrate that, at least for the tested magnetic laminations, the model “(3)-avg” is applicable for switching frequency in the 50–350 kHz range and for 400–2000 Hz fundamental frequency.

It should be considered that for 50 Hz, 200 Hz, and for some of the tested materials also at 400 Hz, over 50 kHz of switching frequency, the specific core losses under PWM are so close to those measured with sinusoidal excitation, which makes the use of the model “(3)-avg” redundant, even if still applicable. As reported in Section VII-A, in its minimal implementation effort, no measurements are required either with a sinusoidal power supply or via a WBG-based PWM inverter, making the estimation method appealing for both practitioners and R&D engineers.

Unquestionably, the weak point of the proposed procedure is that the trends, as shown in Fig. 18, are not known a priori. In fact, even if the four tested materials have very different characteristics in terms of alloy elements, thickness, saturation level, hysteresis loss/eddy current loss ratio, and so on, their coefficients do not surely cover all the possible cases of thin lamination sheets used in high-speed and traction e-motor applications.

When for any reason, the readers do not consider the use of the model coefficients, as shown in Fig. 18, for their specific application, and lamination sheets are available to build a toroidal specimen together with the WBG-based PWM inverter, they can decide to identify the coefficients  $m(f_{fund})$  and  $q(f_{fund})$  directly by tests. However, it should be taken into account that both measuring and data processing steps are quite time-consuming activities, at least if it is desired to try the 25 fundamental/switching frequency combinations, as reported in Table 7. Looking at Fig. 18 once again, it can be observed that the trends of the coefficients  $m_{avg}(f_{fund})$  and  $q_{avg}(f_{fund})$  can be roughly approximated by a second-order polynomial and a straight line, respectively. So, for a fast magnetic material characterization suitable for the loss estimation model “(3)-avg,” the following procedure is suggested.

- 1) Coil the sample for the tests selecting the proper turn number of the windings respecting the voltage and current limitation of the hardware, in particular, at high fundamental frequency. Additionally, it is strongly recommended to measure the impedance of the primary winding with an LCR meter up to 1 MHz. If the inductance is too small or if there are resonances close to the higher switching frequency, try to rewind the sample. A good rule of thumb is not to overlap the magnetizing and sensing windings and arrange the primary winding over almost the entire circumference, concentrating the secondary turns in the free space [6].
- 2) For the selected magnetic material, perform the four tests under the PWM supply identified by the green cells in Table 7. Measure the full spectrum iron losses and the fundamental induced voltage at the secondary winding to determine the fundamental flux frequency to be used in (4).

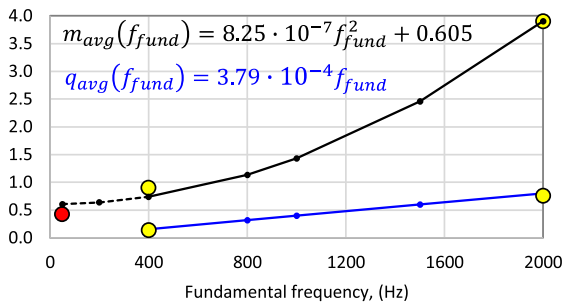


**FIGURE 19.**  $m_{avg}(f_{fund})$  and  $q_{avg}(f_{fund})$  polynomial approximations starting from the four measured values highlighted as yellow dots (the red dot is the  $m_{avg}^* = 0.5$  estimated at low fundamental frequency).

- 3) Estimate the average coefficients  $m$  and  $q$  only at 400 and 2000 Hz for the two considered switching frequencies of 50 and 200 kHz, using the model (3)-avg and a data-fitting algorithm (e.g., the least square method). These values are the four yellow dots in Fig. 19. If no data-fitting tools are available, it is possible to start from the  $m_{avg}^*(f_{fund})$  and  $q_{avg}^*(f_{fund})$  values, as reported in Table 15, manually changing the coefficients  $m$  and  $q$  until a good match between measurements and estimates is obtained.
- 4) Determine the polynomial trends of  $m_{avg}(f_{fund})$  and the  $m_{avg}(f_{fund})$  using a second- and first-order polynomial interpolation, as sketched in Fig. 19. Note that, to determine the second-order polynomial, a third point is needed. It is suggested to use the average  $m_{avg}^* = 0.45$  estimated during the low fundamental frequency test campaign—see Section V-B.

In the future, every time there will be the availability of new stator magnetic cores or toroidal specimens, the above fast characterization procedure will be applied by the authors. This is in order to populate a database of average coefficients  $m(f_{fund})$  and  $q(f_{fund})$ , making the model “(3)-avg” use straightforward and reasonably accurate to compute the specific iron losses at fundamental and switching frequencies well above 400 Hz and 50 kHz, respectively.

## VIII. CONCLUSION

By means of an experimentally based approach, this research work quantifies the specific iron losses of selected laminated magnetic materials excited with PWM voltages synthesized by WBG-based inverters, at high fundamental and switching frequencies. A low-grade and three high-performing magnetic materials typically used for high-speed and automotive applications have been considered to give more generality to the study. The conducted experimental test campaign covers the 50–2000 Hz fundamental frequency range and 1–350 kHz switching frequency range. The test rig and the procedures to get accurate results under these severe excitation conditions are discussed. For two specimens, tests at the highest switching frequencies revealed that the core dimensions and the winding construction play an important role in obtaining reliable measurements. The measurements confirm that the

specific iron losses significantly decrease with the increase of the switching frequency and the impact on the iron losses of different deadtimes is negligible, at least up to 350 kHz. However, even if the switching frequency increase is beneficial for iron losses, it should be verified that the electrical machine is able to withstand ultrafast switching [5].

The collected data have been used to effectively enhance a previously published engineering approach for predicting the iron losses under unipolar sine-triangle PWM at ultrahigh switching frequency case. The employed modulation strategy ensures the elimination of minor hysteresis loops within the main dynamic hysteresis loop. In particular, the eddy current core losses have been modeled by introducing a linear function of the flux density, with a slope and y-intercept depending on the fundamental and switching frequency of the PWM waveform. With the adopted SiC H-bridge and the tested magnetic materials, the unknown parameters of the linear trends have been identified through data fitting. It has been found that, at fundamental frequencies lower than 200 Hz, the coefficients depend essentially on the switching frequency, and they are substantially independent of the material type. Vice-versa, in the range 400–2000 Hz, the model coefficients can be expressed as a function of the fundamental frequency only, but they have to be estimated for each sample. In all the cases, the new estimation model allows for errors close to or lower than 5%, which undoubtedly represents an excellent result. At the end of the study, a design-oriented version of the loss estimation model is presented and critically discussed. In its minimal implementation, this “user-friendly” model does not require any measurement, neither under ac sinusoidal supply nor with PWM inverter. However, for users with the necessary test facilities, a rapid procedure for the magnetic material characterization is proposed to increase confidence in the iron loss computations.

## APPENDIX I

For an ideal unipolar sine-triangle PWM waveform, the  $\alpha$  and  $\beta$  theoretical coefficients depend on the modulation index  $m_i$  and they can be computed as follows.

- 1) H-bridge with 180° shift between the modulations:  $\alpha = 1$  and  $\beta_{180} = 2/\sqrt{\pi \cdot m_i}$ .
- 2) H-bridge with 120° shift in the modulations:  $\alpha = 1$  and  $\beta_{120} = \sqrt[4]{12}/\sqrt{\pi \cdot m_i}$ .

In accordance with the developed models, the coefficient  $\beta^2$  takes into account the eddy current loss increase with sine-triangle PWM excitation. Therefore, the theoretical eddy current loss ratio between the two modulation strategies is

$$\beta_{120}^2/\beta_{180}^2 = 0.866.$$

## APPENDIX II

Figs. 20 and 21 show the amplitude and phase responses of the primary winding impedance of the samples under test. The frequency characterization has been conducted using the IM3536A LCR meter.

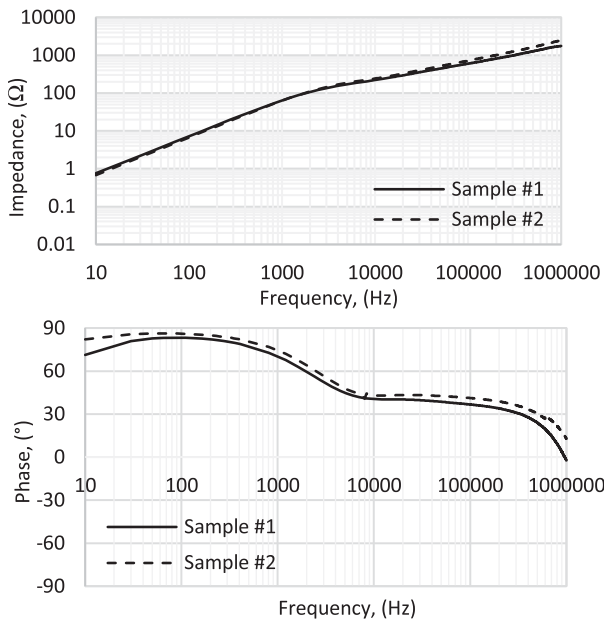


FIGURE 20. Magnitude and phase frequency responses of the primary winding impedance for sample #1 and sample #2.

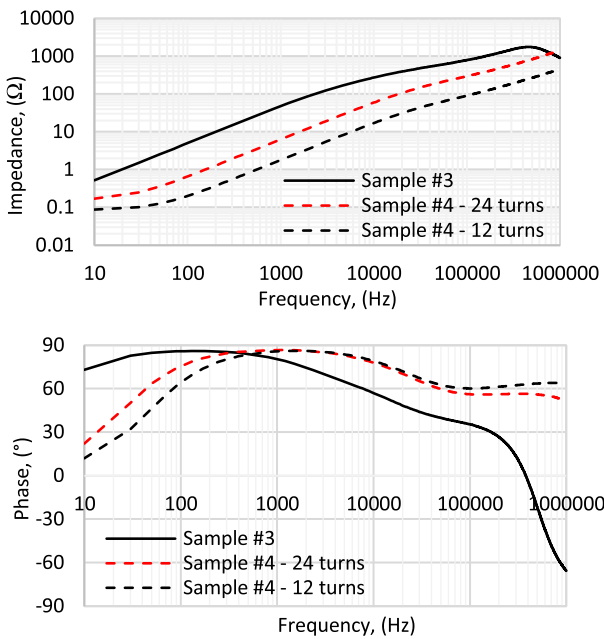


FIGURE 21. Magnitude and phase frequency responses of the primary winding for sample #3 and the two turn number constructions of sample #4.

APPENDIX III

For the considered samples, the average  $m$  and  $q$  values estimated using the theoretical  $\alpha$  and  $\beta$  values are given in the following three tables, while Table 16 lists the estimation errors using the average coefficients of Table XV in the model “(3)-avg.”

TABLE 13. Coefficient  $m_{avg}(f_{fund})$

Sample	Fundamental frequency, (Hz)					
	50	200	400	1000	1500	2000
#1	0.573	0.522	0.902	1.284	2.385	3.897
#2	0.345	0.336	0.524	1.069	2.004	3.625
#3	0.746	0.366	0.264	1.887	3.277	5.609
#4	0.224	0.189	0.279	0.298	0.435	0.679

TABLE 14. Coefficient  $q_{avg}(f_{fund})$

Sample	Fundamental frequency, (Hz)					
	50	200	400	1000	1500	2000
#1	0.185	0.062	0.137	0.432	0.594	0.758
#2	0.169	0.105	0.175	0.299	0.434	0.523
#3	0.000	0.202	0.298	0.276	0.293	0.345
#4	0.000	0.302	0.200	0.240	0.277	0.348

TABLE 15. Coefficients  $m_{avg}^*(f_{fund})$  and  $q_{avg}^*(f_{fund})$

	Fundamental frequency, (Hz)					
	50	200	400	1000	1500	2000
$m(f_{fund})$	0.39	0.42	0.51	1.11	1.94	2.95
$q(f_{fund})$	0.12	0.15	0.19	0.30	0.40	0.50

TABLE 16. Average Percentage Errors in Loss Estimation Using the Practical Model “(3)-Avg” Implemented With the Coefficients in Table 15—Error = 100\*(Computed–Measured)/Measured

$f_{sw}$ , (kHz)	Fundamental frequency, (Hz)				
	400	800	1000	1500	2000
Sample #1					
50	-10.8	-14.3	-13.9	-17.8	-21.0
100	-9.9	-12.2	-10.9	-16.9	-19.5
200	-7.8	-11.9	-10.9	-15.6	-18.6
350	-8.8	-13.8	-11.5	-16.9	-17.3
Sample #2					
50	-1.8	-1.9	-0.5	-4.8	-7.1
100	3.2	0.8	2.1	-1.5	-3.9
200	4.7	2.4	3.8	-0.4	-1.7
350	6.1	2.8	4.2	0.8	-0.5
Sample #3					
50	9.9	n.a.	-18.6	-14.3	-13.4
100	13.8	n.a.	-16.1	-10.6	-10.4
150	15.8	n.a.	-14.3	-9.0	-8.9
200	17.7	n.a.	-13.2	-7.6	-7.7
350	19.1	n.a.	-10.3	-4.4	-3.4
Sample #4					
50	30.6	n.a.	72	142	170
100	37.1	n.a.	75	145	182
150	33.8	n.a.	75	151	185
200	33.2	n.a.	73	144	171
350	27.4	n.a.	63	127	152

ACKNOWLEDGMENT

This article reflects only the authors’ views and opinions and the Ministry cannot be considered responsible for them.

REFERENCES

[1] D. Gerada, A. Mebarki, N. L. Brown, C. Gerada, A. Cavagnino, and A. Boglietti, “High-speed electrical machines: Technologies, trends, and developments,” *IEEE Trans. Ind. Electron.*, vol. 61, no. 6, pp. 2946–2959, Jun. 2014.

[2] S. Li, Y. Li, W. Choi, and B. Sarlioglu, “High-speed electric machines: Challenges and design considerations,” *IEEE Trans. Transp. Electrific.*, vol. 2, no. 1, pp. 2–13, Mar. 2016.



- [3] K. Yamazaki, A. Suzuki, M. Ohto, and T. Takakura, "Harmonic loss and torque analysis of high-speed induction motors," *IEEE Trans. Ind. Appl.*, vol. 48, no. 3, pp. 933–941, May/Jun. 2012.
- [4] A. Morya, M. Moosavi, M. C. Gardner, and H. A. Toliyat, "Applications of wide bandgap (WBG) devices in AC electric drives: A technology status review," in *Proc. 2017 IEEE Int. Electr. Mach. Drives Conf.*, 2017, pp. 1–8.
- [5] G. Scelba, D. Cremente, G. De Donato, S. Vaschetto, E. B. Agamloh, and A. Cavagnino, "Experimental assessment of induction motors fed by sub-MHz-PWM wide band gap inverters," *IEEE Trans. Ind. Appl.*, vol. 58, no. 4, pp. 4461–4473, Jul./Aug. 2022.
- [6] I. Siročić, M. Kovačić, and S. Stipetić, "Methodology and measurement setup for determining PWM contribution to iron loss in laminated ferromagnetic materials," *IEEE Trans. Ind. Appl.*, vol. 57, no. 5, pp. 4796–4804, Sep./Oct. 2021.
- [7] W. Martinez, S. Odawara, and K. Fujisaki, "Iron loss characteristics evaluation using a high-frequency GaN inverter excitation," *IEEE Trans. Mag.*, vol. 53, no. 11, Nov. 2017, Art. no. 1000607.
- [8] M. Oka, H. Kiyotake, M. Enokizono, and D. Wakabayashi, "Iron loss measurements under PWM excitation for ring cores made of ultrathin electrical steel sheets for a stator core," in *Proc. 2020 Int. Conf. Elect. Mach.*, Gothenburg, Sweden, 2020, pp. 2294–2300.
- [9] C. P. Steinmetz, "On the law of hysteresis," *Proc. IEEE*, vol. 71, no. 2, pp. 197–221, Feb. 1984.
- [10] G. Bertotti, "General properties of power losses in soft ferromagnetic materials," *IEEE Trans. Magn.*, vol. 24, no. 1, pp. 621–630, Jan. 1988.
- [11] L. Chang, W. Lee, T. M. Jahns, and K. Rahman, "Investigation and prediction of high-frequency iron loss in lamination steels driven by voltage-source inverters using wide-bandgap switches," *IEEE Trans. Ind. Appl.*, vol. 57, no. 4, pp. 3607–3618, Jul./Aug. 2021.
- [12] L. Chang, T. M. Jahns, and R. Blissenbach, "Characterization and modeling of soft magnetic materials for improved estimation of PWM-induced iron loss," *IEEE Trans. Ind. Appl.*, vol. 56, no. 1, pp. 287–300, Jan./Feb. 2020.
- [13] M. Popescu, D. M. Ionel, A. Boglietti, A. Cavagnino, C. Cossar, and M. I. McGilp, "A general model for estimating the laminated steel losses under PWM voltage supply," *IEEE Trans. Ind. Appl.*, vol. 46, no. 4, pp. 1389–1396, Jul./Aug. 2010.
- [14] Z. Gmyrek, A. Boglietti, and A. Cavagnino, "Iron loss prediction with PWM supply using low- and high-frequency measurements: Analysis and results comparison," *IEEE Trans. Ind. Electron.*, vol. 55, no. 4, pp. 1722–1728, Apr. 2008.
- [15] P. Rasilo, W. Martinez, K. Fujisaki, J. Kyyrä, and A. Ruderman, "Simulink model for PWM-supplied laminated magnetic cores including hysteresis, eddy-current, and excess losses," *IEEE Trans. Power Electron.*, vol. 34, no. 2, pp. 1683–1695, Feb. 2019.
- [16] A. Boglietti, A. Cavagnino, M. Lazzari, and M. Pastorelli, "Predicting iron losses in soft magnetic materials with arbitrary voltage supply: An engineering approach," *IEEE Trans. Mag.*, vol. 39, no. 2, pp. 981–989, Mar. 2003.
- [17] D. Cremente, G. Scelba, G. De Donato, S. Vaschetto, E. Agamloh, and A. Cavagnino, "Measurements and prediction of iron losses in laminated magnetic cores supplied by ultra-high switching frequency PWM," in *Proc. 2022 IEEE Energy Convers. Congr. Expo.*, Detroit, MI, USA, 2022, pp. 1–7.
- [18] *Magnetic Materials—Part 6: Methods of Measurement of the Magnetic Properties of Magnetically Soft Metallic and Powder Materials at Frequencies in the Range 20 Hz to 100 kHz by the Use of Ring Specimens*, Standard IEC 60404-6, IEC, Geneva, Switzerland, May 2018.
- [19] W. Martinez, S. Odawara, and K. Fujisaki, "Sampling frequency influence on magnetic characteristic evaluation under high frequency GaN inverter excitation," in *Proc. IEEE 3rd Int. Future Energy Electron. Conf. ECCE Asia*, 2017, pp. 953–958.
- [20] E. B. Agamloh, A. Cavagnino, and S. Vaschetto, "Standard efficiency determination of induction motors with a PWM inverter source," *IEEE Trans. Ind. Appl.*, vol. 55, no. 1, pp. 398–406, Jan./Feb. 2019.
- [21] D. M. Ionel, M. Popescu, S. J. Dellinger, T. J. E. Miller, R. J. Heideman, and M. I. McGilp, "On the variation with flux and frequency of the core loss coefficients in electrical machines," *IEEE Trans. Ind. Appl.*, vol. 42, no. 3, pp. 658–667, May/Jun. 2006.
- [22] Z. Gmyrek and A. Cavagnino, "Influence of punching, welding, and clamping on magnetic cores of fractional KiloWatt motors," *IEEE Trans. Ind. Appl.*, vol. 54, no. 5, pp. 4123–4132, Sep./Oct. 2018.



**LUIGI DANILLO TORNELLO** (Member, IEEE) received the B.S. and M.S. degrees in electrical engineering and the Ph.D. degree in systems engineering, energy, information technology, and telecommunications from the University of Catania, Catania, Italy, in 2014, 2017, and 2021, respectively.

He is currently a Researcher with Electrical Machines, Drives and Power Electronics Group, University of Catania. His research interests include ac drive control technologies, digital signal

processing techniques, and power semiconductor devices small-signal modeling.

Dr. Tornello was a recipient of the 2018 Third Prize Paper Award from the IES Electrical Machine Technical Committee.



**SILVIO VASCETTO** (Senior Member, IEEE) received the M.Sc. and Ph.D. degrees in electrical engineering from Politecnico di Torino, Torino, Italy, in 2007 and 2011, respectively.

He then joined ABB IEC LV Motors Technology Center, Vittuone, Italy, as an R&D Engineer. From 2012 to 2014, he was with Magna Electronics, Italy, as Electromagnetic Simulation and Motor Design Engineer. He is currently an Associate Professor with Energy Department "G. Ferraris," Politecnico di Torino. His research interests include electromagnetic design, thermal design, and energetic behavior of electrical machines for transportations and high-performance applications. He is an Associate Editor for IEEE TRANSACTIONS ON INDUSTRY APPLICATIONS and IEEE TRANSACTIONS ON ENERGY CONVERSION, and a Special Issues Editor for the *IET Electric Power Applications Journal*.

include electromagnetic design, thermal design, and energetic behavior of electrical machines for transportations and high-performance applications. He is an Associate Editor for IEEE TRANSACTIONS ON INDUSTRY APPLICATIONS and IEEE TRANSACTIONS ON ENERGY CONVERSION, and a Special Issues Editor for the *IET Electric Power Applications Journal*.



**EMMANUEL B. AGAMLOH** (Senior Member, IEEE) received the B.Sc. and M.Sc. degrees in electrical engineering from St. Petersburg State Technical University, St. Petersburg, Russia, in 1992 and 1994, respectively, and the Ph.D. degree in electrical and computer engineering from Oregon State University, Corvallis, OR, USA, in 2005.

He is an Associate Professor with the Department of Electrical and Computer Engineering, Baylor University, Waco, TX, USA. His research interests include electric machine design, analysis,

and testing and renewable energy with application areas, such as industrial, aerospace, transportation, and oil and gas.

Dr. Agamloh was a recipient of two IEEE First Prize Paper Awards for his research. His extensive industry experience includes a 14-year role as a Technical Director of Motors and Drives Laboratory, Advanced Energy Corporation, Raleigh, NC, USA. He was a Technical Paper Review Chair of IEEE TRANSACTIONS ON INDUSTRY APPLICATIONS and a past Chair of the IEEE-IAS Electric Machines Committee. He was the General Chair of the 2022 IEEE Energy Conversion Congress and Exposition held in Detroit, MI, USA.



**GIACOMO SCELBA** (Senior Member, IEEE) was born in Caltagirone, Italy. He received the M.S. and Ph.D. degrees in electrical engineering from the University of Catania, Catania, Italy, in 2002 and 2006, respectively.

He is currently an Associate Professor with the Department of Electrical Electronic and Computer Engineering (DIEEI), University of Catania. He is a co-PI of a collaborative research agreement between the DIEEI and the Department of Astronautical, Electrical and Energy Engineering, Sapienza-University of Rome, Rome, Italy, for research in the field of wide-bandgap-semiconductor-based drives. His current research interests include sensorless control strategies, ac drive control technologies, fault-tolerant motor drives, modeling and control of power converters, and advanced technologies for power electronics' applications.

Dr. Scelba is currently serving as a Secretary of the PELS Technical Committee on Electrical Machines, Drives and Automation. He was a recipient of the 2014 First Prize Paper Award and the 2016 Third Prize Paper Award, both from the IAS Industrial Drives Committee, and the 2018 Third Prize Paper Award from the IES Electrical Machine Technical Committee. He is currently serving as an Associate Editor for IEEE TRANSACTIONS ON INDUSTRY APPLICATIONS.



**GIULIO DE DONATO** (Senior Member, IEEE) was born in Cork, Ireland. He received the M.S. and Ph.D. degrees in electrical engineering from Sapienza-University of Rome, Rome, Italy, in 2003 and 2007, respectively.

He is an Associate Professor with the Department of Astronautical, Electrical and Energy Engineering (DIAEE), Sapienza-University of Rome. He is Co-PI of a collaborative research agreement between the DIAEE and the Department of Electrical, Electronic Engineering, and Computer Science, University of Catania, for research in the field of wide-bandgap semiconductor-based drives. His current research interests include digital control of brushless drives, and analysis and design of permanent magnet machines and wide-bandgap-semiconductor-based power converters.

Dr. De Donato is the Vice Chair of the IAS Electric Machines Committee. He was a recipient of the 2014 First Prize Paper Award and the 2016 Third Prize Paper Award, both from the IAS Industrial Drives Committee. He was acknowledged as an Outstanding Reviewer of IEEE TRANSACTIONS ON POWER ELECTRONICS in 2020. He is an Associate Editor for IEEE TRANSACTIONS ON INDUSTRY APPLICATIONS and IEEE TRANSACTIONS ON POWER ELECTRONICS.



**ANDREA CAVAGNINO** (Fellow, IEEE) was born in Asti, Italy, in 1970. He received the M.Sc. and Ph.D. degrees in electrical engineering from Politecnico di Torino, Torino, Italy, in 1995 and 2000, respectively.

He is a Professor with Politecnico di Torino. He has authored or coauthored more than 250 papers. His research interests include electromagnetic design, thermal design, and energetic behavior of electrical machines. He usually cooperates with factories for a direct technological transfer and he

has been involved in several public and private research projects.

Dr. Cavagnino was a recipient of four Best Paper Awards. He is an Associate Editor for IEEE TRANSACTIONS ON ENERGY CONVERSION, a past Chair of the Electrical Machines Technical Committee of the IEEE Industrial Electronics Society, and a past Associate Editor for IEEE TRANSACTIONS ON INDUSTRIAL ELECTRONICS (TIE) and IEEE TRANSACTIONS ON INDUSTRY APPLICATIONS. He was also a Guest Editor of six Special Sections for IEEE-TIE and Co-Editor-in-Chief for a Special Issue for IEEE-TEC. He was a Technical Program Chair of the IEEE-IEMDC 2015, IEEE-ECCE 2022, and IEEE-ECCE 2025 conferences. He is a reviewer for several IEEE Transactions and other international journals and conferences.

Open Access funding provided by 'Politecnico di Torino' within the CRUI CARE Agreement